analytical chemistry

Article

Cite This: Anal. Chem. 2019, 91, 823−829

pubs.acs.org/ac

Dual-Aptamer-Conjugated Molecular Modulator for Detecting Bioactive Metal Ions and Inhibiting Metal-Mediated Protein Aggregation

Jie Wang,[†,§] Yingqian Wang,[†,§] Xiaoxia Hu,[†,§] Chunli Zhu,[†] Qinqin Ma,[†] Ling Liang,[‡] Zhihao Li,[†] and Quan Yuan*[,†]

[†]Key Laboratory of Analytical Chemistry for Biology and Medicine (Ministry of Education), College of Chemistry and Molecular Sciences, Wuhan University, Wuhan 430072, China

[‡]Molecular Science and Biomedicine Laboratory, State Key Laboratory of Chemo/Biosensing and Chemometrics, College of Chemistry and Chemical Engineering and College of Biology, Collaborative Innovation Center for Chemistry and Molecular Medicine, Hunan University, Changsha 410082, China

Supporting Information

ABSTRACT: Bioactive metal ions play important roles in both physiological and pathological processes. Developing biosensing probes for bioactive metal ion detection can contribute to fields including disease diagnosis and therapy and studying the mechanisms of biological activities. In this work, we designed a dual-aptamer-conjugated molecular modulator that can detect Zn^{2+} and further inhibit Zn^{2+}-induced amyloid β (Aβ) aggregation. The molecular modulator is able to selectively target Aβ species and block Zn^{2+} due to the specific recognition capability of aptamers. With the binding of Zn^{2+}, the fluorescence signal of this molecular modulator is restored, thus allowing for Zn^{2+} detection. More importantly, this molecular modulator can inhibit the generation of Zn^{2+}-triggered Aβ aggregates due to the trapping of Zn^{2+} around Aβ species. Circular dichroism measurements reveal that the dual-aptamer-conjugated molecular modulator prevents the conformational transition of the Aβ monomer from a random coil to a β-sheet. Furthermore, after treating with the molecular modulator, no Aβ aggregate is observed in the Aβ solution with added Zn^{2+}, demonstrating that Aβ aggregation is successfully inhibited by this molecular modulator. Our approach provides a promising tool for detecting bioactive metal ions and studying the molecular mechanisms behind life activities.

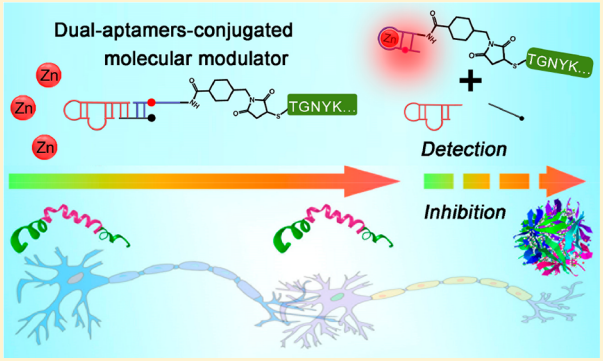

Protein misfolding leads to a series of neurodegenerative disorders that feature tissue deposition protein aggregates rich in β sheets.[1,2] Alzheimer's disease (AD) is one of the most common age-related neurodegenerative disorders in which abundant amyloid β (Aβ) aggregates generate neuritic plaques in the brain.[3] According to the amyloid cascade hypothesis, the accumulation of Aβ aggregates in plaques is the primary driving force for AD pathogenesis.[4−6] In amyloid neurotoxic plaques, the homeostasis of metal ions, particularly zinc ion (Zn^{2+}), is seriously damaged.[7] According to previous studies, Zn^{2+} is an important trigger source to induce Aβ misfolding and aggregation, suggesting the crucial role of Zn^{2+} in the onset of amyloidosis pathology in AD.[8−10] The low level of Zn^{2+} (1−10 nM) in cerebrospinal fluid is essential for neural function in a healthy brain, and this concentration of Zn^{2+} is too low to induce the formation of misfolded protein aggregates. Generally, 0.1−1 μM Zn^{2+} is needed for significant Zn^{2+}−Aβ binding,[11] whereas previous studies reported that Zn^{2+} with concentrations up to micromolar can trigger the misfolding and aggregation of Aβ. Also, some neurons contain Zn^{2+} with concentrations up to dozens of micromoles.[9,12,13] The above facts indicate that detection of Zn^{2+} is important for determining Zn^{2+}−Aβ-associated pathological pathways in AD. More importantly, because a high concentration of Zn^{2+} is the essential trigger of the misfolding and aggregation of Aβ, trapping of Zn^{2+} that is around Aβ species can serve as an efficient way to inhibit the generation of Aβ aggregates. Therefore, rational design of Zn^{2+}-targeted biosensing probe is crucial for understanding Zn^{2+}−Aβ-related neuropathology and for further inhibition of Zn^{2+}-induced protein aggregation.

Given the recognized interactions of metal ions with Aβ peptide,[14] metal chelating agents could potentially play an important role in lowering Zn^{2+}-mediated Aβ aggregation and neurotoxicity. Metal chelators such as clioquinol (CQ) can decrease Aβ aggregation,[15,16] but CQ is a nonspecific chelator and cannot detect the level of Zn^{2+}.[17] In addition, metal

Received: July 4, 2018
Accepted: December 3, 2018
Published: December 3, 2018

DOI: 10.1021/acs.analchem.8b03007
Anal. Chem. 2019, 91, 823−829

chelators may lead to adverse side effects, such as subacute myelo-optic neuropathy, thus limiting their long-term clinical applications.[18] Aptamers are short oligonucleotide strands that can specifically recognize and bind to various targets,[19] such as metal ions,[20,21] small molecules,[22] cells,[23,24] and even tissues.[25] They can be engineered for a particular application and can be conveniently used to design various probes for biosensing and therapy.[26−28] In this regard, aptamers are ideal candidates for design of a Zn^{2+}-specific probe for Zn^{2+} detection. Furthermore, aptamers elicit little or no immunogenicity in therapeutic applications.[29,30] Recently, a DNA aptamer called Zn6m2 was developed to specifically recognize Zn^{2+} with a K_d value of 15 μM.[31] An aptamer-based biosensing probe would open new opportunities for detecting Zn^{2+} and further inhibiting Zn^{2+}-induced protein aggregation.

Endowing the biosensing probe with an Aβ-targeted moiety can further promote the specific interaction between the biosensing probe and Zn^{2+} around Aβ species for more efficient inhibition of Aβ aggregation.[32,33] The Aβ-specific aptamer β55, reported by Farrar et al., exhibits high specificity and affinity to Aβ species.[34] Herein, we developed a dual-aptamer-conjugated molecular modulator for detecting Zn^{2+} and further inhibiting Zn^{2+}-mediated Aβ aggregation. As shown in Scheme 1, we designed a dual-aptamer-conjugated molecular modulator able to detect Zn^{2+} and simultaneously inhibit Zn^{2+}-induced Aβ aggregation. This molecular modulator has four domains: an Aβ-specific aptamer β55, a Texas Red-labeled Zn^{2+}-specific aptamer (Texas Red-labeled-Zn6m2), a peptide called TGN[35] and a black hole quencher-2 (BHQ-2)-labeled complementary DNA. Specifically, β55 is employed as the targeting molecule for Aβ species, and Texas Red-labeled Zn6m2 is used as the recognition element for Zn^{2+}. First, a TGN peptide that can penetrate the blood-brain barrier is covalently linked with Texas Red-labeled-Zn6m2 to construct a TGN-Zn6m2 conjugate. Next, the BHQ-2-labeled complementary DNA ties the β55 and TGN-Zn6m2 conjugate via complementary base pairing. This molecular modulator can specifically target Aβ species and bind to the surrounding Zn^{2+}. With the trapping of Zn^{2+}, the Zn^{2+}-specific aptamer undergoes a conformational change, causing the release of BHQ-2-labeled complementary DNA. Thus, the fluorescence signal of this molecular modulator is recovered, signaling detection of Zn^{2+}. More importantly, this molecular modulator can inhibit the generation of Zn^{2+}-triggered Aβ aggregates due to the trapping of Zn^{2+} around Aβ species. These functions make the dual-aptamer-conjugated molecular modulator a promising platform for detecting Zn^{2+} and manipulating Aβ aggregation, which can open new possibilities for understanding the mechanisms of metal-related protein aggregation and AD therapy.

Scheme 1. Schematic Representation of the Dual-Aptamer-Conjugated Molecular Modulator for Detection of Zn^{2+} and Simultaneous Inhibition of Zn^{2+}-Induced Aβ Aggregation

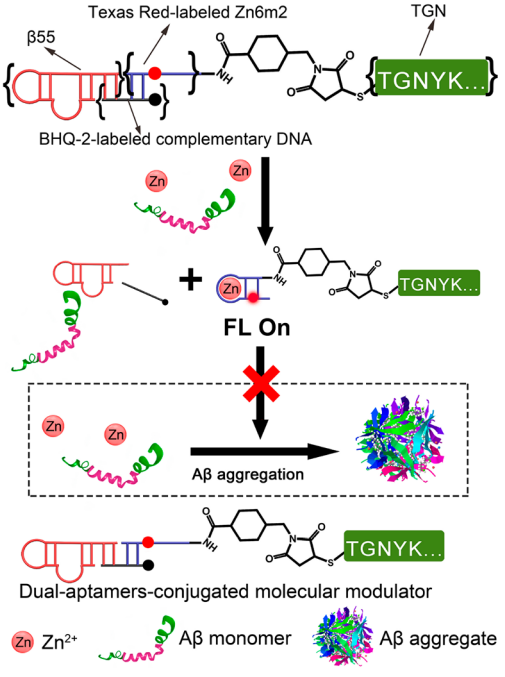

EXPERIMENTAL SECTION

Preparation of Dual-Aptamer-Conjugated Molecular Modulator. The TGN-Zn6m2 conjugate was first prepared by linking the TGN peptide with Texas Red-labeled Zn6m2. In detail, the 3′ amino group of the oligonucleotide was reacted with 1.5 equiv of sulfosuccinimidyl-4-(*N*-maleimidomethyl)-cyclohexane-1-carboxylate (Sulfo-SMCC) in PB buffer (50 mM, pH 7.4) for 1 h. Then, the maleimide-activated oligonucleotide was reacted with the thiol (−SH) containing TGN peptide at a molar ratio of 1:2 at room temperature overnight. The resultant TGN-Zn6m2 conjugates were passed twice through an ultrafilter (3 kDa, Millipore) with ddH_2O to exchange the buffer and remove the free peptides. The obtained TGN-Zn6m2 conjugates were then mixed with 2 equiv of BHQ-2-labeled complementary DNA and equivalent β55 in PBS buffer (10 mM, 137 mM NaCl, pH 7.4). The mixture was heated to 75 °C and maintained for 3 min. Next, this mixture was cooled to room temperature and stored in the dark for 12 h to allow complete hybridization. The dual-aptamer-conjugated molecular modulator was obtained by ultrafiltration (30 kDa, Millipore) with ddH_2O twice to remove the unreacted oligonucleotides.

Preparation of Dual-Aptamer-Conjugated DNA Molecule. The Texas Red-labeled Zn6m2 was first mixed with 2 equiv BHQ-2-labeled complementary DNA and equivalent β55 in PBS buffer (10 mM, 137 mM NaCl, pH 7.4). The mixture was heated to 75 °C and maintained for 3 min. Next, this mixture was cooled to room temperature, and stored in the dark for 12 h to allow complete hybridization. The dual-aptamer-conjugated DNA molecules were finally obtained by ultrafiltration (30 kDa, Millipore) with ddH_2O twice to remove the unreacted oligonucleotides.

Pretreatment of Commercial Aβ1-42. First, the commercial Aβ1-42 peptide was dissolved in hexafluoroisopropanol (HFIP) (1 mM), and the solution was incubated for 1 h at room temperature. Then, the solution was divided into portions and evaporated under vacuum. The obtained Aβ1-42 monomer was stored at −80 °C.

Colocalization Assay of Dual-Aptamer-Conjugated Molecular Modulator and FAM-Labeled Aβ1-42. LSCM was applied to observe the colocalization of the molecular modulator and Aβ. Texas Red-labeled molecular modulator (2 nM, 100 μL) was incubated with 100 μL of FAM-labeled Aβ (2 nM) for 1 h at room temperature. In addition, Texas Red-labeled TGN-Zn6m2 conjugate with no β55 was used as the control group. In detail, 100 μL of Texas Red-labeled TGN-Zn6m2 conjugate (2 nM) was incubated with 100 μL of FAM-

DOI: 10.1021/acs.analchem.8b03007
Anal. Chem. 2019, 91, 823−829

labeled Aβ (2 nM) for 1 h at room temperature. Then, 30 μL of each solution was dropped into separate Petri dishes, and a coverslip was carefully placed on the liquid drop. A 586 nm laser was equipped for the excitation of Texas Red, and a 495 nm laser was used for the excitation of FAM. The images from the Texas Red channel and FAM channel were obtained. All of the images were acquired using a 100× oil objective.

Detection of Zn^{2+}. To investigate the feasibility of the dual-aptamer-conjugated molecular modulator for Zn^{2+} detection, the fluorescence signals were obtained in various concentrations of Zn^{2+}. Various concentrations of Zn^{2+} were added to solutions of Aβ1-42 peptide (10 μM). The mixtures were then incubated at 37 °C for 1 h in the dark. The fluorescence intensity was finally recorded under 586 nm excitation. For comparison, after treatment of the molecular modulator with Zn^{2+} in PBS buffer (10 mM, 137 mM NaCl, pH 7.4), the fluorescence intensity was also obtained.

Formation of the Zn^{2+}-Induced Aβ Aggregate. First, Aβ1-42 stock solution was prepared by dissolving Aβ1-42 peptide in HEPES buffer (20 mM, 100 mM NaCl, pH 7.4). This solution was sonicated in an ice bath for 10 min and then filtered through a 0.22 μm filter to minimize the number of preformed aggregates. Second, stock solution of Zn^{2+} (200 μM) was prepared by dissolving $ZnCl_2$ in H_2O. Finally, a Zn^{2+} solution was added to the Aβ1-42 solution, giving final concentrations of 10 μM for Aβ1-42 and 20 μM for Zn^{2+}. The mixtures were incubated at 37 °C for 2 h.

Study of Conformational Transformation. CD measurements were carried out to study the conformational transformation of Aβ1-42 peptide. Three samples were prepared to conduct the CD experiment: fresh Aβ1-42, Aβ1-42 incubated with Zn^{2+} (20 μM) for 2 h, Aβ1-42 incubated with Zn^{2+} (20 μM), and molecular modulator for 2 h. CD spectra were collected with a Jasco-810 spectropolarimeter using a 1 mm path quartz cell. Each sample was scanned over the wavelength range from 200 to 260 nm. The DNA background was subtracted out when the Zn^{2+} containing Aβ solution was treated molecular modulator.

Real-Time Monitoring of the Inhibition of Aβ Aggregation by Light Scattering Measurement. The aggregation process can be monitored by the intensity of scattered light from the sample cell using a fluorescence spectrometer. Typically, two kinds of samples were prepared as follows: 20 μL of Aβ1-42 solution (10 μM) was added to 180 μL of Zn^{2+} solution (10 μM), 20 μL of Aβ1-42 solution (10 μM) was added to 180 μL of a solution containing 10 μM Zn^{2+} and 10 μM molecular modulator. The scattering intensities were recorded over time on a fluorescence spectrometer. Each sample was monitored in a 200 μL quartz fluorescence cuvette using a fluorescence spectrometer to record the scattered light. The excitation and emission wavelengths were both set at 650 nm. The excitation slit and emission slit were both set at 5.0 nm. The emission was detected at a right angle relative to the excitation light.

Morphology Analysis by Transmission Electron Microscopy (TEM). Both the formation of Aβ aggregates and the inhibition of aggregation were confirmed by electron microscopy of negatively stained samples. Three kinds of samples were prepared as follows: fresh Aβ1-42 (2 μM), 2 μL of Aβ1-42 (20 μM) incubated with 18 μL of Zn^{2+} for 2 h, 2 μL of Aβ1-42 (20 μM) incubated with 18 μL of Zn^{2+}, and molecular modulator for 2 h. Ten microliters of prepared sample was first dropped on carbon-coated copper grids and left for 1−2 min at room temperature. Then, the sample on the copper grid was stained with 2% (w/v) phosphotungstic acid for another 1 min. The samples were examined with a transmission electron microscope (Hitachi, Tokyo, Japan) operating at 100 kV.

Topography Analysis by AFM. To observe the topography of Aβ peptide from the horizontal and vertical angles, AFM measurements were carried out. Three kinds of samples were prepared following the procedure described above for TEM. Then, the sample was spin-coated on muscovite mica. Data were acquired in the tapping mode using an atomic force microscope with Bruker Multimode 8.

Observation of the Inhibition of Zn^{2+}-Induced Aβ Aggregation with LSCM. Four kinds of samples were prepared as follows: fresh FAM-labeled Aβ1-42 (2 μM), 2 μL of FAM-labeled Aβ1-42 monomer (20 μM) treated with 18 μL of Zn^{2+} for 2 h, 2 μL of FAM-labeled Aβ1-42 monomer treated with 18 μL of molecular modulator for 2 h, 2 μL of FAM-labeled Aβ1-42 monomer (20 μM) treated with 18 μL of Zn^{2+} and molecular modulator for 2 h. A 30 μL aliquot of each sample was dropped on a Petri dish, and a coverslip was placed on the liquid drop. The images from the Texas Red channel and FAM channel were captured with excitation by a 586 nm laser and a 495 nm laser, respectively. All of the images were obtained using a 100× oil objective.

RESULTS AND DISCUSSION

As shown in Figure 1a, Texas Red label on the molecular modulator was chosen as the energy donor, while BHQ-2 acted as the energy acceptor. Förster resonance energy transfer (FRET) between Texas Red and BHQ-2 thus leads to fluorescence quenching. As shown in Figure 1b, fluorescence intensity of Texas Red gradually decreases with increasing concentration of BHQ-2-labeled complementary DNA. The normalized intensity shows a complementary DNA-dependent decrease of fluorescence (Figure 1c), indicating the effective intramolecular FRET between Texas Red and BHQ-2. The fluorescent colocalization assay of the dual-aptamer-conjugated molecular modulator and Aβ species was performed by laser scanning confocal microscopy (LSCM). To make the dual-aptamer-conjugated molecular modulator fluorescent, we removed the BHQ-2 label. As shown in Figure 1d, when the fluorescein amidite (FAM)-labeled Aβ was incubated with the dual-aptamer-conjugated molecular modulator, both strong red and green fluorescence are obtained. Obviously, the merged image shows bright yellow fluorescence, indicating that the molecular modulator colocalizes well with Aβ. When FAM-labeled Aβ was incubated with the TGN-Zn6m2 conjugate having no β55, strong red and green fluorescence are also observed from the confocal images (Figure 1e). However, as shown in the overlapped image in Figure 1e, there is no overlapping fluorescence between the TGN-Zn6m2 conjugate and Aβ because the red and green fluorescence are separate. These colocalization results in LSCM studies confirm that the dual-aptamer-conjugated molecular modulator can specifically bind to Aβ. In addition, the specificity of the molecular modulator demonstrates that β55 was successfully integrated with TGN-Zn6m2 conjugate through the complementary DNA.

The working principle for detection of Zn^{2+} by the dual-aptamer-conjugated molecular modulator is presented in Figure 2a. The fluorescence of the molecular modulator is quenched due to the close proximity between Texas Red and

DOI: 10.1021/acs.analchem.8b03007
Anal. Chem. 2019, 91, 823−829

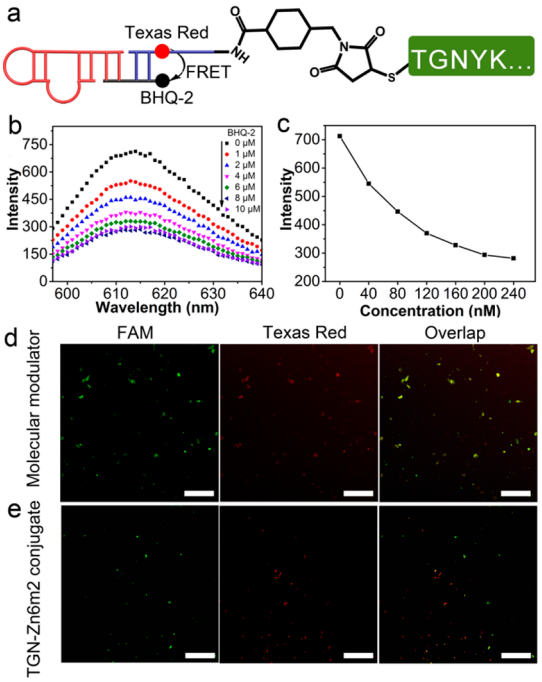

Figure 1. (a) Schematic illustration of the dual-aptamer-conjugated molecular modulator. (b) The fluorescence intensity of Texas Red in response to various concentrations of BHQ-2-labeled complementary DNA. (c) The relationship between the fluorescence intensity of Texas Red and the concentration of BHQ-2-labeled complementary DNA. (d) Colocalization of FAM-labeled Aβ1-42 and molecular modulator. The image captured from the FAM channel represents the FAM-labeled Aβ, and the image captured from the Texas Red channel represents the molecular modulator. The colocalization coefficient is 83.83%. (e) Colocalization of FAM-labeled Aβ1-42 and TGN-Zn6m2 conjugate. The image captured from the FAM channel represents the FAM-labeled Aβ, and the image captured from the Texas Red channel represents the TGN-Zn6m2 conjugate. The TGN-Zn6m2 conjugate refers to the modulator without the β55 aptamer and BHQ-2 label. The colocalization coefficient is 52.51%. Scale bars are 10 μm.

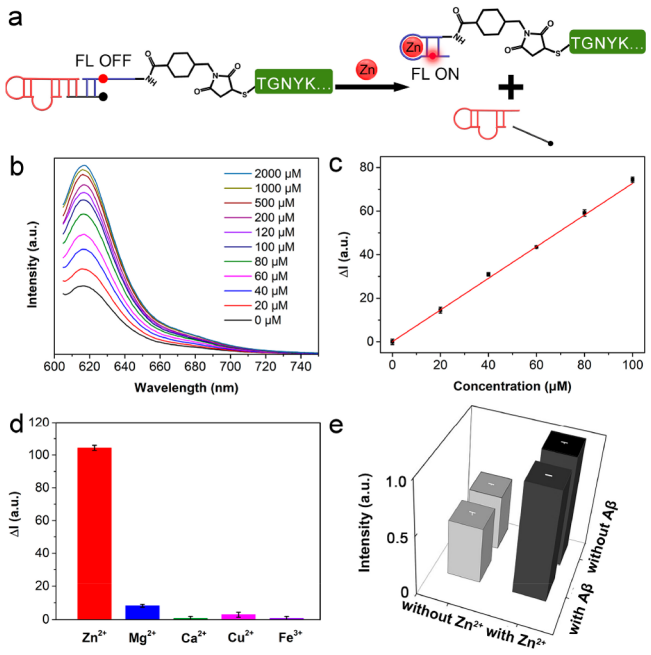

Figure 2. (a) Schematic illustration of the molecular modulator for Zn^{2+} detection. (b) The fluorescence intensity of the solution containing the modulator (2 μM) and Aβ1-42 (10 μM) in the presence of Zn^{2+} with different concentrations. (c) Plot of the enhanced fluorescence intensity (ΔI) versus Zn^{2+} concentration. (d) The enhanced fluorescence intensity (ΔI) of the solution containing the modulator (2 μM) and Aβ1-42 (10 μM) in the presence of Zn^{2+} (2 mM), Mg^{2+} (2 mM), Ca^{2+} (2 mM), Cu^{2+} (2 mM), and Fe^{3+} (2 mM), respectively. (e) The normalized fluorescence intensity of the modulator in the presence of Zn^{2+} (100 μM) with and without Aβ1-42 (10 μM).

BHQ-2. When treated with Zn^{2+}, the molecular modulator can specifically recognize and bind to Zn^{2+}. In this case, the Zn6m2 can undergo a conformational change, so that the 5′ end of the aptamer associates with the Zn^{2+} and the BHQ-2-labeled complementary DNA is released, leading to fluorescence recovery. As shown in Figure 2b, the fluorescence intensity of the biosensing system containing modulator (2 μM) progressively increases with increasing concentrations of Zn^{2+} from 0 to 2000 μM in Aβ solution. The normalized fluorescence intensity is found to be linear in the Zn^{2+} concentration range from 0 to 100 μM (Figure 2c). Thus, the molecular modulator exhibits a Zn^{2+} concentration-dependent increase in fluorescence. The limit of detection toward Zn^{2+} was determined to be 4.9 μM. Moreover, Figure 2d shows that the molecular modulator displays good selectivity for Zn^{2+} against other physiological relevant metal ions. In addition, similar fluorescence recovery is obtained in solution either with or without Aβ (Figure 2e), indicating that Aβ exhibits no side effects on Zn^{2+} detection. As a result, the modulator can serve as a robust probe for detection of Zn^{2+} in Aβ solution.

To verify the effect of Zn^{2+} in acceleration conversion of Aβ monomers into Aβ aggregates, the commonly used Thioflavin T (ThT) fluorescence assay was employed. ThT is an extrinsic fluorescent dye which can specifically bind to amyloid aggregates, and its fluorescence intensity can be largely enhanced after binding.[36,37] The ThT fluorescence assay was carried out to examine the evolution of Aβ aggregation in the presence of Zn^{2+} at various aging times. As shown in Figure 3a, ThT fluorescence largely increased after incubation with Zn^{2+} for the first half hour, indicating the rapid aggregation of Aβ. Then, the ThT fluorescence increased more gradually as time progressed to reach the maximum fluorescence intensity. Importantly, the maximum ThT fluorescence intensity from Aβ1-42 solution without Zn^{2+} was lower than that from Aβ1-42 solution with the addition of Zn^{2+} (Figure 3b). These results demonstrate that Zn^{2+} is an important trigger for Aβ aggregation. The dual-aptamer-conjugated molecular modulator was then applied as an inhibitor to prevent Zn^{2+}-induced Aβ aggregation. Figure 3c illustrates the light scattering technique for real-time monitoring the process of Aβ aggregation. Because Aβ monomers are soluble in solution, the scattering signal is weak. In the presence of Zn^{2+}, Aβ monomers undergo misfolding and aggregation. The soluble Aβ monomers thus convert into insoluble Aβ aggregates, leading to a significant enhancement of the scattering signal. When an Aβ solution also containing Zn^{2+} was treated with the molecular modulator, the misfolding and aggregation of Aβ monomer was prevented because the molecular modulator sequestered the Zn^{2+}. Thus, the scattering signal of the monomer solution remained weak. As presented in Figure 3d, Aβ1-42 solution with added Zn^{2+} showed strong light scattering, verifying the formation of Aβ aggregates. When

DOI: 10.1021/acs.analchem.8b03007
Anal. Chem. 2019, 91, 823−829

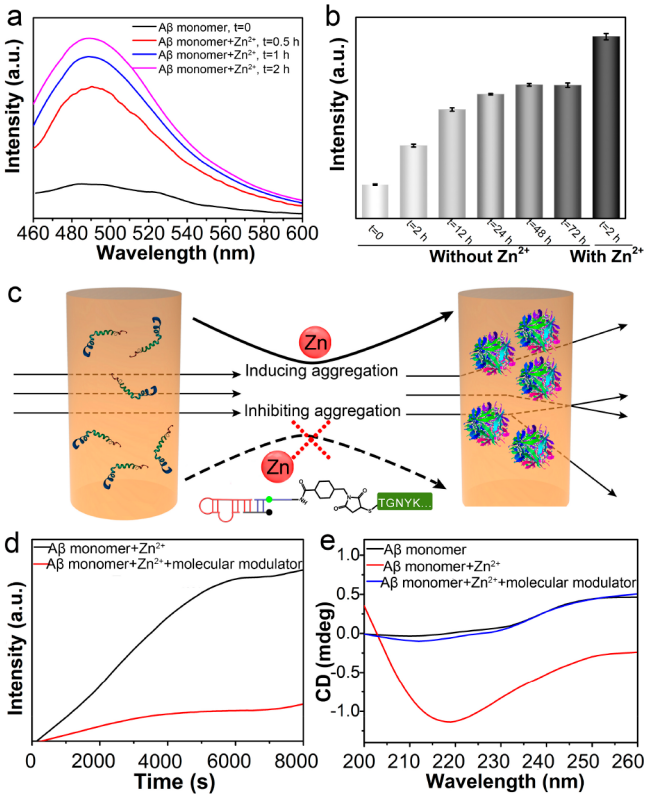

Figure 3. (a) ThT fluorescence assay of Aβ1-42 incubated with Zn^{2+} at various aging time. (b) Normalized ThT fluorescence intensity of Aβ1-42 incubated with and without Zn^{2+}. (c) Schematic illustration of the inhibition of Zn^{2+}-induced aggregation of Aβ. (d) Real-time light scattering spectra of solutions containing Zn^{2+} and Aβ1-42 (with and without molecular modulator). (e) CD spectra of fresh Aβ1-42, Aβ1-42 incubated with Zn^{2+}, and Aβ1-42 incubated with Zn^{2+} and molecular modulator.

Aβ1-42 solution containing Zn^{2+} was treated with the molecular modulator, the final scattering signal was much lower than that of the sample treated with Zn^{2+} alone, suggesting the effective sequestration of Zn^{2+} and inhibition of Aβ aggregation. According to previous studies, the secondary structural transition of Aβ from random-coil to β-sheet is observed during the process of Aβ aggregation.[38,39] Circular dichroism (CD) studies were therefore carried out to study the conformational transformation of Aβ. As shown in Figure 3e, the freshly prepared Aβ1-42 shows a random coil structure. In contrast, when Aβ1-42 was incubated with Zn^{2+}, it exhibited a stronger negative peak at 217 nm. This negative band at 217 nm is a characteristic of Aβ aggregation, mainly due to the β-sheet secondary structure.[40] The change of CD spectra indicates that Zn^{2+} triggers the conformation conversion of Aβ monomer. Upon the addition of molecular modulator, the CD result is in accordance with that of the fresh Aβ1-42, thus suggesting that the structural change of Aβ1-42 was hindered. These CD studies demonstrate that the molecular modulator can inhibit the structural transition of Aβ1-42 from native random coil to the neurotoxic β-sheet conformation.

As illustrated in Figure 4a, the misfolding and aggregation of Aβ can be induced by Zn^{2+}. In the presence of the molecular modulator, the Zn^{2+}-mediated Aβ aggregation can be inhibited, thus enabling Aβ monomer to remain in its native structure and morphology. The morphologies of Aβ1-42 under various conditions were observed by negative-stain transmission

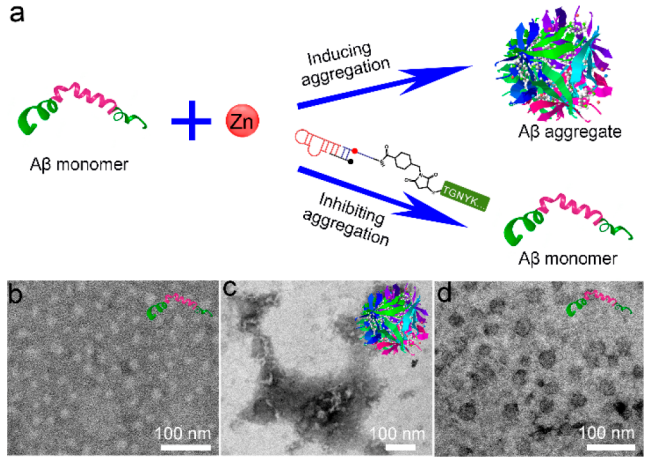

Figure 4. (a) Inhibition of Zn^{2+}-induced Aβ aggregation. (b) TEM image of fresh Aβ1-42. (c) TEM image of Aβ1-42 incubated with Zn^{2+}. (d) TEM image of Aβ1-42 incubated with Zn^{2+} and molecular modulator.

electron microscopy (TEM). The fresh Aβ1-42 was observed as a little dot, which corresponds to the morphology of Aβ monomer[9] (Figure 4b). But when Aβ1-42 was incubated with Zn^{2+}, large aggregates of irregular shapes with sizes of hundreds of nanometers were observed (Figure 4c and Figure S10). These large aggregates are proved to be insoluble nonfibrillar Aβ aggregates.[9,38] Their characteristic spherical domain texture indicates that they were formed by incorporation of small spherical aggregates. In contrast, in the presence of molecular modulator, some little dots were observed, which were much smaller than the Zn^{2+}-induced Aβ aggregates (Figure 4d). These unstructured and small-sized Aβ species are known to be less toxic or nontoxic.[41] As a result, this molecular modulator can be used as an inhibiting tool specific for Zn^{2+}-triggered Aβ aggregation, thereby reducing Zn^{2+}-related neurotoxicity in AD.

Because AFM has excellent horizontal and vertical resolution, it is a useful tool for visualizing Aβ species.[40,42] Figure 5a shows a representative AFM topography image of Aβ1-42 treated with Zn^{2+}, and huge Aβ aggregates are observed. These Aβ aggregates appear as plaques of diameters up to 400 nm and heights from 8 to 37 nm (Figure 5b). As for the Aβ1-42 treated with molecular modulator, small spherical structures are observed (Figure 5c). The line cuts verify that these Aβ species have heights of less than 2 nm (Figure 5d). These features are attributed to a single (0.75 nm) or double (1.5 nm) layer of Aβ1-42,[43] indicating the inhibition of misfolding and aggregation of Aβ monomers. These results further demonstrate that the dual-aptamer-conjugated molecular modulator provides significantly enhanced inhibitory capacity toward Zn^{2+}-induced Aβ aggregation.

The inhibition of Zn^{2+}-induced Aβ aggregation was further verified by LSCM. For freshly prepared FAM-labeled Aβ1-42, no fluorescence was observed in the Texas Red channel, and dotted green fluorescence is observed from the FAM channel (Figure 6a). The dotted green fluorescence is derived from the fresh FAM-labeled Aβ1-42, indicating that the freshly prepared Aβ1-42 is of small size. As shown in Figure 6b, after treating the FAM-labeled Aβ1-42 with Zn^{2+}, the Texas Red channel remains black. But, a large number of huge plaques with green fluorescence are observed, verifying that Aβ aggregation can be induced by Zn^{2+}. When FAM-labeled Aβ1-42 was incubated

DOI: 10.1021/acs.analchem.8b03007
Anal. Chem. 2019, 91, 823−829

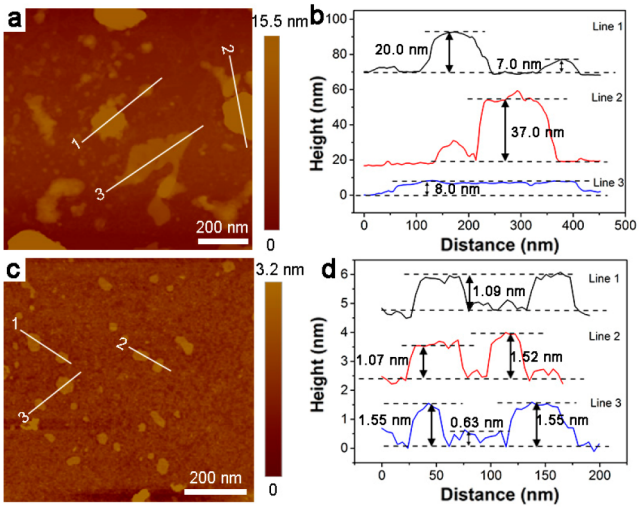

Figure 5. (a) AFM image and (b) height distributions of the line cuts of Aβ1-42 treated with Zn^{2+}. (c) AFM image and (d) height distributions of the line cuts of Aβ1-42 treated with Zn^{2+} and molecular modulator.

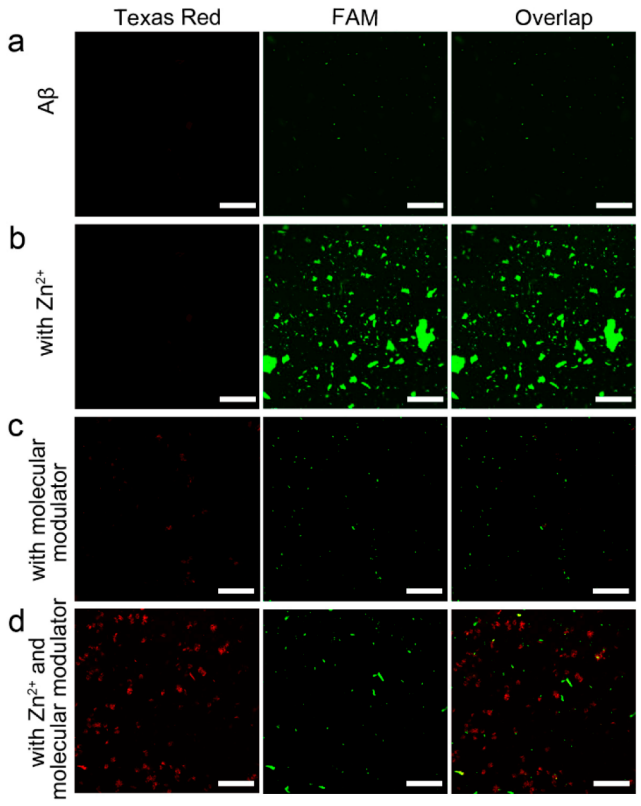

Figure 6. Confocal images of (a) freshly prepared FAM-labeled Aβ1-42, (b) FAM-labeled Aβ1-42 incubated with Zn^{2+}, (c) FAM-labeled Aβ1-42 incubated with molecular modulator, and (d) FAM-labeled Aβ1-42 incubated with Zn^{2+} and molecular modulator. Scale bars are 10 μm.

with the molecular modulator, weak red fluorescence can be observed from the Texas Red channel (Figure 6c). This weak red fluorescence is attributed to the FRET process between the Texas Red and BHQ-2. In addition, dotted green fluorescence is visualized from the FAM channel (Figure 6c). As presented in Figure 6d, when the molecular modulator was introduced into an Aβ1-42 solution with added Zn^{2+}, bright red fluorescence is observed, indicating that Zn^{2+} caused the release of BHQ-2-labeled complementary DNA from the molecular modulator. Thus, Zn^{2+} around Aβ species can be visualized with the red fluorescence signal output. Importantly, dotted green fluorescence is observed in the FAM channel, indicating that the molecular modulator is an effective inhibitor for Zn^{2+}-triggered aggregation of Aβ. Combining the results from Figures 6c and d, we conclude that the molecular modulator can act as a useful probe for Zn^{2+} detection. Importantly, the fluorescence results from the FAM channel demonstrate that the molecular modulator is also an efficient inhibitor for Zn^{2+}-induced aggregation of Aβ. Taken together, this dual-aptamer-conjugated molecular modulator exhibits outstanding performance in evaluation of Zn^{2+} in Aβ species as well as inhibition of Aβ aggregation.

CONCLUSION

In summary, we designed a dual-aptamer-conjugated molecular modulator that can detect Zn^{2+} and can further inhibit Zn^{2+}-mediated Aβ aggregation. The fluorescence of this molecular modulator can be efficiently restored after binding to Zn^{2+}, thus allowing for Zn^{2+} detection. Importantly, the molecular modulator can specifically recognize Aβ species and sequester the surrounding Zn^{2+}, thus inhibiting the generation of Zn^{2+}-triggered Aβ aggregates. The molecular modulator described here can provide valuable information for understanding Zn^{2+}−Aβ-related neuropathology and exhibits great potential in inhibiting Aβ aggregation. We anticipate that this molecular modulator will find broad application in the study of metal ion detection and regulation of metal-induced protein aggregation.

ASSOCIATED CONTENT

Supporting Information

The Supporting Information is available free of charge on the ACS Publications website at DOI: 10.1021/acs.analchem.8b03007.

Instrumentation information and supplementary figures (PDF)

AUTHOR INFORMATION

Corresponding Author

*E-mail: yuanquan@whu.edu.cn.

ORCID

Jie Wang: 0000-0003-4170-8470

Quan Yuan: 0000-0002-3085-431X

Author Contributions

§J.W., Y.W., and X.H. contributed equally.

Notes

The authors declare no competing financial interest.

ACKNOWLEDGMENTS

This work was supported by the National Natural Science Foundation of China (Grant 21675120), National Key R&D Program of China (Grants 2017YFA0208000 and 2016YFF0100800), National Basic Research Program of China (973 Program, Grant 2015CB932600), the National Postdoctoral Program for Innovative Talents (Grant BX20180223), Project funded by China Postdoctoral Science Foundation (Grant 2018M640726), Ten Thousand Talents Program for Young Talents, and the Start-up Research Fund for Q.Y. (Grants 531107050973 and 531109010053).

DOI: 10.1021/acs.analchem.8b03007
Anal. Chem. 2019, 91, 823−829

REFERENCES

(1) Pepys, M. B. *Philos. Trans. R. Soc., B* **2001**, *356*, 203−211.
(2) Pepys, M. B. *Annu. Rev. Med.* **2006**, *57*, 223−241.
(3) Hardy, J.; Selkoe, D. J. *Science* **2002**, *297*, 353−356.
(4) Tanzi, R. E.; Bertram, L. *Cell* **2005**, *120*, 545−555.
(5) LaFerla, F. M.; Green, K. N.; Oddo, S. *Nat. Rev. Neurosci.* **2007**, *8*, 499−509.
(6) Truex, N. L.; Wang, Y.; Nowick, J. S. *J. Am. Chem. Soc.* **2016**, *138*, 13882−13890.
(7) Bush, A. I. *Trends Neurosci.* **2003**, *26*, 207−214.
(8) Huang, X.; Atwood, C. S.; Hartshorn, M. A.; Multhaup, G.; Goldstein, L. E.; Scarpa, R. C.; Cuajungco, M. P.; Gray, D. N.; Lim, J.; Moir, R. D.; Tanzi, R. E.; Bush, A. I. *Biochemistry* **1999**, *38*, 7609−7616.
(9) Noy, D.; Solomonov, I.; Sinkevich, O.; Arad, T.; Kjaer, K.; Sagi, I. *J. Am. Chem. Soc.* **2008**, *130*, 1376−1383.
(10) Miller, Y.; Ma, B.; Nussinov, R. *Proc. Natl. Acad. Sci. U. S. A.* **2010**, *107*, 9490−9495.
(11) Smith, M. A.; Harris, P. L. R.; Sayre, L. M.; Perry, G. *Proc. Natl. Acad. Sci. U. S. A.* **1997**, *94*, 9866−9868.
(12) Frederickson, C. J.; Koh, J. Y.; Bush, A. I. *Nat. Rev. Neurosci.* **2005**, *6*, 449−462.
(13) Sensi, S. L.; Paoletti, P.; Bush, A. I.; Sekler, I. *Nat. Rev. Neurosci.* **2009**, *10*, 780−791.
(14) Liu, J.; Chakraborty, S.; Hosseinzadeh, P.; Yu, Y.; Tian, S.; Petrik, I.; Bhagi, A.; Lu, Y. *Chem. Rev.* **2014**, *114*, 4366−4469.
(15) Barnham, K. J.; Masters, C. L.; Bush, A. I. *Nat. Rev. Drug Discovery* **2004**, *3*, 205−214.
(16) Rodríguez-Rodríguez, C.; de Groot, N. S.; Rimola, A.; Álvarez-Larena, Á.; Lloveras, V.; Vidal-Gancedo, J.; Ventura, S.; Vendrell, J.; Sodupe, M.; González-Duarte, P. *J. Am. Chem. Soc.* **2009**, *131*, 1436−1451.
(17) Cahoon, L. *Nat. Med.* **2009**, *15*, 356−359.
(18) Ritchie, C. W.; Bush, A. I.; Mackinnon, A.; Macfarlane, S.; Mastwyk, M.; MacGregor, L.; Carrington, D. *Arch. Neurol.* **2003**, *60*, 1685−1691.
(19) Li, F.; Zhang, H.; Wang, Z.; Newbigging, A. M.; Reid, M. S.; Li, X.-F.; Le, X. C. *Anal. Chem.* **2015**, *87*, 274−292.
(20) Zhou, W.; Ding, J.; Liu, J. *Nucleic Acids Res.* **2016**, *44*, 10377−10385.
(21) Fan, H.; Zhang, X.; Lu, Y. *Sci. China: Chem.* **2017**, *60*, 591−601.
(22) Gu, C.; Lan, T.; Shi, H.; Lu, Y. *Anal. Chem.* **2015**, *87*, 7676−7682.
(23) Huang, Y. F.; Chang, H. T.; Tan, W. *Anal. Chem.* **2008**, *80*, 567−572.
(24) Song, J.; Lv, F.; Yang, G.; Liu, L.; Yang, Q.; Wang, S. *Chem. Commun.* **2012**, *48*, 7465−7467.
(25) Zhou, W.; Huang, P. J. J.; Ding, J.; Liu, J. *Analyst* **2014**, *139*, 2627−2640.
(26) Xiang, Y.; Lu, Y. *Inorg. Chem.* **2014**, *53*, 1925−1942.
(27) Shao, Y.; Jia, H.; Cao, T.; Liu, D. *Acc. Chem. Res.* **2017**, *50*, 659−668.
(28) Zhang, H.; Chao, J.; Pan, D.; Liu, H.; Qiang, Y.; Liu, K.; Cui, C.; Chen, J.; Huang, Q.; Hu, J.; Wang, L.; Huang, W.; Shi, Y.; Fan, C. *Nat. Commun.* **2017**, *8*, 14738.
(29) Shangguan, D.; Li, Y.; Tang, Z.; Cao, Z. C.; Chen, H. W.; Mallikaratchy, P.; Sefah, K.; Yang, C. J.; Tan, W. *Proc. Natl. Acad. Sci. U. S. A.* **2006**, *103*, 11838−11843.
(30) Kumar, A.; Kim, S.; Nam, J. M. *J. Am. Chem. Soc.* **2016**, *138*, 14509−14525.
(31) Rajendran, M.; Ellington, A. D. *Anal. Bioanal. Chem.* **2008**, *390*, 1067−1075.
(32) Lee, J. Y.; Cole, T. B.; Palmiter, R. D.; Suh, S. W.; Koh, J. Y. *Proc. Natl. Acad. Sci. U. S. A.* **2002**, *99*, 7705−7710.
(33) Beck, M. W.; Oh, S. B.; Kerr, R. A.; Lee, H. J.; Kim, S. H.; Kim, S.; Jang, M.; Ruotolo, B. T.; Lee, J. Y.; Lim, M. H. *Chem. Sci.* **2015**, *6*, 1879−1886.
(34) Farrar, C. T.; William, C. M.; Hudry, E.; Hashimoto, T.; Hyman, B. T. *PLoS One* **2014**, *9*, e89901.
(35) Zhang, C.; Wan, X.; Zheng, X.; Shao, X.; Liu, Q.; Zhang, Q.; Qian, Y. *Biomaterials* **2014**, *35*, 456−465.
(36) Li, M.; Howson, S. E.; Dong, K.; Gao, N.; Ren, J.; Scott, P.; Qu, X. *J. Am. Chem. Soc.* **2014**, *136*, 11655−11663.
(37) Yee, A. W.; Moulin, M.; Breteau, N.; Haertlein, M.; Mitchell, E. P.; Cooper, J. B.; Erba, E. B.; Forsyth, V. T. *Angew. Chem., Int. Ed.* **2016**, *55*, 9292−9296.
(38) Dong, J.; Shokes, J. E.; Scott, R. A.; Lynn, D. G. *J. Am. Chem. Soc.* **2006**, *128*, 3540−3542.
(39) Abelein, A.; Jarvet, J.; Barth, A.; Gräslund, A.; Danielsson, J. *J. Am. Chem. Soc.* **2016**, *138*, 6893−6902.
(40) Taniguchi, A.; Sasaki, D.; Shiohara, A.; Iwatsubo, T.; Tomita, T.; Sohma, Y.; Kanai, M. *Angew. Chem., Int. Ed.* **2014**, *53*, 1382−1385.
(41) Hyung, S. J.; DeToma, A. S.; Brender, J. R.; Lee, S.; Vivekanandan, S.; Kochi, A.; Choi, J. S.; Ramamoorthy, A.; Ruotolo, B. T.; Lim, M. H. *Proc. Natl. Acad. Sci. U. S. A.* **2013**, *110*, 3743−3748.
(42) Qiang, Q.; Kelley, K.; Tycko, R. *J. Am. Chem. Soc.* **2013**, *135*, 6860−6871.
(43) Economou, N. J.; Giammona, M. J.; Do, T. D.; Zheng, X.; Teplow, D. B.; Buratto, S. K.; Bowers, M. T. *J. Am. Chem. Soc.* **2016**, *138*, 1772−1775.

DOI: 10.1021/acs.analchem.8b03007
Anal. Chem. 2019, 91, 823−829